Semiclassical dynamics of circular-orbit Rydberg wave packets

Mark Mallalieu and C. R. Stroud, Jr.
The Institute of Optics, University of Rochester, Rochester, New York 14627
(Received 15 November 1993)

A semiclassical propagator is applied to describe the dynamics of circular-orbit wave packets which are initially well localized in three dimensions. A sum over classical Kepler trajectories for the wave-packet autocorrelation function is obtained which is extremely accurate well past the classical regime of the evolution of the wave packet. The nonclassical nature of the wave-packet evolution at long times is associated with the interference between amplitudes from classical paths at different energies. The time scale of the wave-packet revivals is related to the shearing rate of the corresponding classical ensemble.

PACS number(s): 03.65.Sq, 31.50.+w, 32.80.Rm

I. INTRODUCTION

A clear understanding of the relationship between the classical trajectories of the Kepler problem and the dynamics of quasiclassical states of hydrogen has eluded physicists for decades. This is in spite of the fact that the relationship between the quantized energy levels and certain Kepler orbits was properly formulated when Bohr developed his model of the atom, even before the birth of modern quantum mechanics. The earliest attempt to clarify the meaning of the classical limit for spatially well-localized quasiclassical states was by Schrödinger, who tried to adapt his theory of "coherent" states for the harmonic oscillator to hydrogen and failed [1]. This was more than a failure of technique, as certain assumptions about the transition from quantum to classical mechanics were implicit in the attempt itself.

In recent years there have been renewed efforts in this direction which use a variety of quasiclassical or coherent states [2–11]. Some approaches to building such states use sophisticated generalized coherent-state theories to find a superposition of eigenstates [2–4], and others are based more on considerations involved in experimentally creating such states with the use of short laser pulses [5–9]. The ideal in all of these approaches is the creation of a state that is well-localized in position and moves along a Kepler ellipse [4,10,11] much as a classical particle would, with the only difference between the wave packet and the classical particle being limits set by the uncertainty principle. This picture holds for short times, but as the wave packet evolves it first decays and later exhibits nonclassical revivals. These features of the wave-packet evolution are easily explained [11–13] in terms of the evolution of the eigenstate superposition coefficients. However, the possible connection of these phenomena with the underlying classical dynamics remains obscure because the representation of the wave-packet evolution via a superposition of eigenstates is not natural from the point of view of classical correspondence.

A resolution of this difficulty is provided here with the use of a semiclassical method that is suited to the study of time-dependent dynamical systems. This approach has been developed by Tomsovic and Heller [14,15], who have applied it successfully even when the classical mechanics is chaotic. This method is a refinement of the Gaussian wave-packet theory that has been used by Heller [16] and Littlejohn [17] in their studies of the relationship between quantum dynamics and classical phase space. The technique is based upon an extension of the Van Vleck propagator [18] due to Gutzwiller [19]. This semiclassical propagator is the WKB approximation to the Feynman propagator. It maintains the sum-over-paths view of quantum mechanics due to Feynman, but in this case only the classical paths are included in the sum. This allows for a relatively simple explanation of the nonclassical regime of the wave-packet evolution, when the wave-packet probability distribution differs in significant ways from the corresponding classical ensemble of trajectories. At such times, the difference between the two distributions can be explained by the interference between many possible classical path amplitudes.

We begin in Sec. II by describing the Van Vleck–Gutzwiller propagator and outlining Tomsovic and Heller's approach to its use in the evaluation of wave-packet correlation functions. The particular states to which we apply this method are Rydberg wave packets that are localized in all three dimensions on a circular Kepler orbit. These states were first introduced by Brown [10], and later were studied in more detail by Gaeta and Stroud [11]. We discuss these states and their evolution in Sec. III. Following that, the classical ensemble that corresponds to this wave packet will be discussed in Sec. IV. There the orbits appropriate for evaluation of the semiclassical approximation to the wave packet's autocorrelation function will be found. In Sec. V we apply this semiclassical technique to the evolution of a three-dimensional wave packet. This is the first step in the application of these methods to closely related nonintegrable problems, such as the diamagnetic Kepler problem and the microwave ionization of hydrogen, which will require multidimensional treatments. Related to the present work is that of Barnes *et al.* [20] for the one-dimensional hydrogen atom.

II. SEMICLASSICAL CORRELATION FUNCTIONS

A semiclassical theory based upon classical trajectories provides a representation that is useful for studying the evolution of a state which is initially a well-localized wave packet. This representation is more intuitive than a conventional energy eigenstate expansion which may involve hundreds or thousands of states that have little direct connection to the dynamics. Such wave-packet states are commonly excited by short laser pulses or collisions, and are of increasing interest in atomic and molecular physics.

Quite often highly excited systems have classical counterparts which are interesting in their own right, because of the chaotic or nonintegrable character of their evolution. The semiclassical method of this section was originally developed by Tomsovic and Heller [14] to address the issues involved in the relationship between the classical dynamics of nonintegrable systems and their quantum mechanical counterparts. The more important details of the technique are given here; complete treatments of its fundamentals can be found in the works of Heller and co-workers [14,16] and Gutzwiller [19,21].

The starting point is the Green's function representation of the quantum mechanical propagator, $K(\mathbf{q},\mathbf{q}';t)$, which takes amplitudes from position $\mathbf{q}'$ to position $\mathbf{q}$ in time t. The evolution of the wave function can be approximated with the semiclassical form of this propagator, $K_{\rm sc}$, by

$$\psi(\mathbf{q},t) \approx \int d\mathbf{q}'\, K_{\rm sc}(\mathbf{q},\mathbf{q}';t)\,\psi(\mathbf{q}',0)\ . \tag{1}$$

This is the ideal equation to solve, because any physical quantity of interest can be calculated once the wave function is known. However, quite often it is just as useful to have the solution to correlation functions of the form

$$\begin{aligned} C_{ba}(t) &= \int d\mathbf{q}\,\psi_b^*(\mathbf{q},0)\,\psi_a(\mathbf{q},t) \\ &\approx \iint d\mathbf{q}\,d\mathbf{q}'\,\psi_b^*(\mathbf{q},0) K_{\rm sc}(\mathbf{q},\mathbf{q}';t)\,\psi_a(\mathbf{q}',0)\ . \end{aligned} \tag{2}$$

For example, the ionization signal of wave packets excited by a short laser pulse in a pump-probe experiment can be directly related to this type of correlation function. In addition, the time-evolved wave function as represented in Eq. (1) can be indirectly solved by expanding it in a basis, and the evolution of the coefficients in the expansion can be found [15] from equations of the form of Eq. (2). As we will show, the application of the semiclassical propagator is considerably simplified when it is used to evaluate the correlation function of two well-localized wave packets. Before discussing this aspect of the method, it is necessary to describe the semiclassical approximation in more detail.

The fundamental semiclassical tool needed for either Eq. (1) or (2) is the Van Vleck–Gutzwiller (VVG) propagator

$$\begin{aligned} K_{\rm sc}(\mathbf{q},\mathbf{q}';t) = \left(\frac{1}{2\pi i\hbar}\right)^{N/2} \sum_j \left|\det\left(\frac{\partial^2 R_j(\mathbf{q},\mathbf{q}';t)}{\partial\mathbf{q}\partial\mathbf{q}'}\right)\right|^{1/2} \\ \times \exp\left(\frac{i}{\hbar}R_j(\mathbf{q},\mathbf{q}';t) - i\frac{\pi}{2}\mu_j\right), \end{aligned} \tag{3}$$

which can be derived from the Feynman propagator [22]. This semiclassical propagator represents a superposition of classical path amplitudes. The sum over j is for all trajectories in the N-dimensional space which travel from $\mathbf{q}'$ to $\mathbf{q}$ in time t. The phase of the jth contribution depends on the classical action R_j and the Maslov index μ_j of the corresponding classical path. The Maslov (or Morse) index is related to the number of conjugate points (focal points, caustics, etc.) of the trajectory in question. The *full* action R_j is also known as Hamilton's principal function [21,23]. It is given by the time integral of the Lagrangian $\mathcal{L}$ along the jth trajectory,

$$R_j(\mathbf{q},\mathbf{q}';t) = \int_0^t dt'\mathcal{L}(\dot{\mathbf{q}},\mathbf{q},t')\Big|_j = S_j(\mathbf{q},\mathbf{q}';E_j) - E_j t\ . \tag{4}$$

Here we have assumed a conservative system. The *reduced* action S_j, which is given by

$$S_j(\mathbf{q},\mathbf{q}',E_j) = \int_0^t dt'\,\mathbf{p}_j\cdot\dot{\mathbf{q}} = \int_{\mathbf{q}'}^{\mathbf{q}} \mathbf{p}_j\cdot d\mathbf{q}''\ , \tag{5}$$

commonly appears in other semiclassical theories. We use the same notation for these classical actions as Gutzwiller in his textbook [21], where he gives an excellent exposition of the classical underpinnings of $K_{\rm sc}(\mathbf{q},\mathbf{q}';t)$ and related semiclassical Green's functions. Heller [14,16] and others designate the full action by S instead of R. As much previous work in atomic physics [6] has used semiclassical theories based on the reduced action S, rather than the full action R, we choose to conform to Gutzwiller's notation.

The magnitude of each contribution in Eq. (3) is equal to the square root of a classical density which depends on the stability of the trajectory. This can be seen by introducing the inverse of the matrix in the determinant in Eq. (3),

$$-\frac{\partial^2 R}{\partial\mathbf{q}\partial\mathbf{q}'} = \frac{\partial\mathbf{p}'}{\partial\mathbf{q}} \equiv \mathbf{U}^{-1}\ . \tag{6}$$

The meaning of this matrix is best understood by considering trajectories which start at $\mathbf{q}'$ at time $t=0$ with a small difference in initial momentum $\delta\mathbf{p}'$ from a trajectory which reaches $\mathbf{q}$ at time t. The difference in their final position from $\mathbf{q}$, given by the increment $\delta\mathbf{q}$, depends upon the matrix $\mathbf{U}$ by $\delta\mathbf{q} = \mathbf{U}\delta\mathbf{p}'$. So the magnitude of each contribution in Eq. (3) depends on the stability of the corresponding trajectory, or the spread of the trajectories nearby, and represents a density of trajectories. As the propagator is to be used in an integral, this density is a weighting term for a differential volume of trajectories starting in a volume $d\mathbf{q}'$ about $\mathbf{q}'$ and ending in the volume $d\mathbf{q}$ about $\mathbf{q}$. Thus, the role this density plays is

similar to the role that the density of states plays in solid state theory or the study of ionization into a continuum. The nature of the matrix **U** and its connection with the Maslov index μ is discussed in more detail in Gutzwiller's book [21].

There are two difficulties one encounters when applying the VVG propagator in the integrals of Eqs. (1) and (2). For any arbitrary pair of end points $(\mathbf{q}', \mathbf{q})$, it is quite possible for the number of trajectories involved to become unmanageably large or even infinite. Furthermore, the integration to be performed is highly oscillatory and therefore not amenable to a numerical computation. Tomsovic and Heller [14] have recently resolved these two problems by considering application of the VVG propagator (3) to the correlation functions of well-localized Gaussian wave packets.

The first step is to recognize that the classical ensemble ρ_a associated with a well-localized wave packet ψ_a is easily determined from its probability distributions in position and momentum space. For the propagation of such a wave packet, it makes sense to restrict the trajectories used for the VVG propagator to those with initial conditions determined by ρ_a. If the correlation function of $\psi_a(t)$ with another well-localized wave packet $\psi_b(0)$ is under consideration, the relevant trajectories are found from the subset of the classical ensemble ρ_a which evolves in time t to become a subset of the classical ensemble ρ_b corresponding to ψ_b. This concept is illustrated in Fig. 1. Classical trajectories not in this subensemble $\rho_a(t) \cap \rho_b(0)$ will give contributions to the VVG propagator which are highly oscillatory with respect to the integrations over initial and final wave functions for the correlation function. These contributions will average out, leaving the contributions from the trajectories given by $\rho_a(t) \cap \rho_b(0)$ to dominate the result. This can be likened to a "filtering" of the VVG propagator by the wave packets [14,16].

The example in Fig. 1 illustrates a situation at short times for which there is only one contribution for every pair $(\mathbf{q}', \mathbf{q})$, with the possible exception of contributions from trajectories outside of $\rho_a(t) \cap \rho_b(0)$ which are ignored henceforth. At long times, the ensemble $\rho_a(t)$ will most likely be spread out over a large region of space. In general, it will fold over upon itself or "mix" in ways that depend upon the nature of the dynamics (integrable, chaotic, etc.). When this happens, there will be more than one contribution in the semiclassical sum for most pairs of initial and final positions $(\mathbf{q}', \mathbf{q})$, even with the restriction to physically relevant trajectories. A proper understanding of the dynamics allows one to organize the set $\rho_a(t) \cap \rho_b(0)$ according to its topological properties. Consider two pairs of points $(\mathbf{q}_1', \mathbf{q}_1)$ and $(\mathbf{q}_2', \mathbf{q}_2)$, where the primed coordinates are both located near the center of one wave packet and the unprimed coordinates are near the center of the other. In the sum over trajectories for the VVG propagator, for every trajectory labeled by j_1 for the first pair of end points, there is a trajectory labeled by j_2 for the second pair which is a smooth deformation of the first trajectory. If a sensible scheme has been developed for the labeling of the trajectories, then $j_1 = j_2 = k$, and the summation index in Eq. (3) is independent of $(\mathbf{q}', \mathbf{q})$, over the range of coordinates where the wave packets have significant amplitudes. This defines a *partitioning* of the ensemble $\rho_a(t) \cap \rho_b(0)$.

The partitioning of the ensemble allows the order of integration and summation to be interchanged when the VVG propagator (3) is inserted into Eq. (2), resulting in the partitioned semiclassical correlation function

$$C_{ba}(t) \approx \sum_k C_{ba}^k(t) = \sum_k \iint d\mathbf{q}\, d\mathbf{q}'\, \psi_b^*(\mathbf{q}, 0)\, K_{\mathrm{sc}}^k(\mathbf{q}, \mathbf{q}'; t)\, \psi_a(\mathbf{q}', 0)\ . \tag{7}$$

If the partitioning is done correctly, the value of the VVG propagator for all of the members of the kth partition can be approximated by a Taylor series expansion of the action R about that of a representative trajectory in that partition. This *reference* trajectory must be chosen carefully, in order to minimize the error in the phase of the partition's contribution [14]. The expansion of $R_k(\mathbf{q}, \mathbf{q}'; t)$ about the initial and final positions $(\mathbf{q}_0, \mathbf{q}_t)$ of the reference trajectory is carried out to second order in $\mathbf{q}' - \mathbf{q}_0$ and $\mathbf{q} - \mathbf{q}_t$ in the Appendix. The first-order terms depend only upon the initial and final momenta

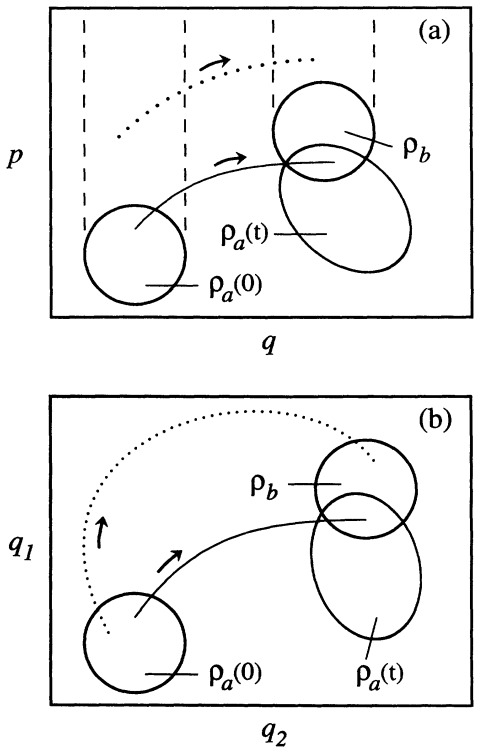

FIG. 1. Set of trajectories relevant to semiclassical correlation function, shown in (a) phase space, (b) configuration space. The solid line indicates the trajectory of a representative member of the set $\rho_a(t) \cap \rho_b(0)$. The dotted line indicates a trajectory which is not a member of either ρ_a or ρ_b at any time, but has initial and final positions within the projection onto configuration space of ρ_a and ρ_b, respectively, and so would be needed for a direct evaluation of the VVG propagator.

of the reference trajectory. The second-order terms depend upon the elements of the matrix given in Eq. (6), evaluated for the reference trajectory. It often proves convenient to solve for those matrix elements with the use of the stability matrix defined by

$$\begin{pmatrix} \delta\mathbf{q}_t \\ \delta\mathbf{p}_t \end{pmatrix} = \mathbf{M}_t \begin{pmatrix} \delta\mathbf{q}_0 \\ \delta\mathbf{p}_0 \end{pmatrix}, \tag{8}$$

where $(\delta\mathbf{q}_0, \delta\mathbf{p}_0)$ are small deviations about the initial position and momenta of the reference trajectory, and $(\delta\mathbf{q}_t, \delta\mathbf{p}_t)$ are the resulting deviations at the final time t. The relationship between the matrices given in Eqs. (6) and (8) is given in the Appendix. The stability matrix defined by Eq. (8) represents a linearization of the dynamics for trajectories near the reference trajectory, and is the key to accounting for the contributions of an entire partition with a single reference trajectory. Tomsovic and Heller [14] discuss this linearized dynamics in more detail, particularly with regards to chaotic classical systems. The linearized dynamics near circular Kepler trajectories will be given in Sec. IV.

The expansion of the action R_k out to second order turns the exponential in Eq. (3) into a complex Gaussian. The use of this linearized semiclassical propagator allows for an analytical solution to the integral for C_{ba}^k in Eq. (7) when ψ_a and ψ_b are Gaussian as well. More details of this procedure are given in the Appendix. The use of the resulting solution for C_{ba}^k in Eq. (7) yields a sum with the form

$$C_{ba}(t) = \sum_k \zeta_k \exp\left(\frac{i}{\hbar} R_k^0\right),$$

where R_k^0 is the classical action of the kth reference trajectory. The complex amplitude ζ_k depends on the properties of the reference trajectory and the parameters of the initial and final Gaussians. The beauty of this approach is that now the semiclassical solution for the correlation function has been reduced to a sum over reference trajectories, which are a much smaller set of trajectories than the total number of physically relevant trajectories, much less the total number of classical trajectories which would contribute to the VVG propagator in a formal sense. Furthermore, for integrable systems such as the Kepler problem, the classical parameters needed for this solution to the partitioned correlation function can be found explicitly. As will be shown in Sec. V, this makes it possible to understand the long-time behavior of these wave packets in different terms than we use when we examine the exact quantum mechanical expression involving the quantized energy levels.

III. CIRCULAR-ORBIT WAVE PACKETS

Now that the semiclassical approach has been explained, it is time to discuss the Rydberg wave packets to which it will be applied. The circular-orbit wave packets [10,11] can be considered to be among the most classical of the Rydberg wave packets localized on a Kepler ellipse [4]. This is because all of the quantum numbers are large for the states involved in the superposition, which are known as the circular-orbit, or aligned, hydrogenic eigenfunctions ($m = l = n - 1$). The wave-packet state is a Gaussian superposition of these eigenstates over a range of energies,

$$\psi(\mathbf{r}, t) = (\pi\sigma_n^2)^{-1/4} \sum_n \exp\left(-\frac{(n-\overline{n})^2}{2\sigma_n^2} - i\omega_n t\right) \Phi_n(\mathbf{r}), \tag{9}$$

where the mean energy of the wave packet $\overline{\omega}$ depends on $\overline{n}$. The energies of the states are given by $\omega_n = -1/2n^2$ in atomic units, which are used throughout this paper. It has been shown by Gaeta and Stroud [11] that this state has uncertainty products approaching their minimum values in all three dimensions. It can be shown [10] that the Gaussian wave packet

$$\psi_{\mathrm{wp}}(\mathbf{r}) = N_g \exp\left[i\overline{n}(\phi - \overline{\phi})\right] \times \exp\left(-\frac{(r-\overline{r})^2}{2\sigma_r^2} - \frac{(\theta-\overline{\theta})^2}{2\sigma_\theta^2} - \frac{(\phi-\overline{\phi})^2}{2\sigma_\phi^2}\right) \tag{10}$$

is a good approximation to the circular-orbit quasiclassical state in Eq. (9) at $t = 0$. The polar coordinates used in Eq. (10) have the z axis for the polar axis. The parameters of the Gaussian assume that $\sigma_n \ll \overline{n}$, and are given by $\sigma_r^2 = 4\overline{n}^2\sigma_n^2$, $\sigma_\theta^2 = 1/\overline{n}$, $\sigma_\phi = 1/\sigma_n$, $\overline{r} = \overline{n}^2$, $\overline{\theta} = \pi/2$, and $\overline{\phi} = 0$.

These circular-orbit wave packets were first studied by Brown [10], who considered their dynamics only for relatively short times. The long-time dynamics of these states were studied by Gaeta and Stroud [11], who have made a videotape of the full evolution which displays all of the interesting features of these wave packets. The state in Eqs. (9) and (10) represents an electron initially localized with near minimum uncertainty about $(\overline{r}, \overline{\theta}, \overline{\phi}) = (\overline{n}^2, \pi/2, 0)$. As this state evolves in time it remains localized in the x-y plane on the circle $r = \overline{r}$, so we need only to consider the ϕ dependence as a function of time. For the first few classical orbit periods, the state remains fairly well-localized around $\phi(t) = \overline{\phi} + \omega_{\mathrm{cl}} t$, as if it were a classical electron with $m = l = \overline{n}$. The wave packet spreads in ϕ, but this can be understood from the classical dynamics by considering the spreading of an equivalent ensemble of particles.

As the wave packet evolves further, it spreads completely around the circle and then its evolution develops nonclassical features. At certain critical times in this quantum regime of evolution, wave-packet structures known as fractional revivals form. When this occurs the wave function consists of a set of localized wave packets [11,12], each identical to the initial state, which are distributed symmetrically in ϕ about the circle $r = \overline{r}$. This curious behavior contrasts with that of the corresponding classical ensemble at these times, which will be more or less evenly distributed about a circular annulus centered at $\overline{r}$. It would appear that classical correspondence completely breaks down at this point.

As was shown in the last section, the Van Vleck–Gutzwiller propagator provides a simple way to understand this discrepancy. With this propagator, when more than one classical path is involved there will be interference between their amplitudes. Thus, the quantum features of the wave-packet evolution can be given a classical "grounding," providing a more complete appreciation of the correspondence between the classical and quantum dynamics of this system. Therefore, it is necessary to find the proper partitioning scheme for the classical ensemble relevant to these Rydberg wave packets, and to choose the appropriate reference trajectories. The next section discusses these trajectories and their properties, which will be used in Sec. V to calculate the semiclassical autocorrelation function of the circular-orbit Rydberg wave packet.

IV. CIRCULAR-ORBIT CLASSICAL DYNAMICS

The importance of the circular orbits for the Rydberg wave packet in Eq. (10) can be seen from its probability distribution. From the Gaussian form of its coordinate representation, it is clear that the members of the relevant classical ensemble have initial positions near $(r,\theta,\phi) = (\overline{r},\pi/2,0)$. It is easy to see that the circular-orbit wave packet's momentum space representation will be centered at $(p_r,p_\theta,p_\phi) = (0,0,\overline{n})$, keeping in mind that $\hbar = 1$ in atomic units. All trajectories with these conditions on their initial position and momenta are circular or nearly circular Kepler trajectories oriented close to the x-y plane. This set will be referred to as the *circular-orbit ensemble*, even though only a subset of this ensemble is composed of strictly circular trajectories.

The semiclassical evaluation of the autocorrelation function for the wave packet requires a partitioning of this ensemble and a determination of the reference trajectories according to the scheme outlined in Sec. II. The key step is to recognize that all Kepler orbits with the same energy will have the same period regardless of ellipticity or orientation. In atomic units the energy and period are given by

$$E = -\frac{1}{2n^2} \quad , \quad T = 2\pi n^3 \ , \tag{11}$$

and depend only upon one action variable, n, which corresponds to the principal quantum number in the quantized hydrogen atom. If an initially well-localized ensemble of trajectories with the same energy, but varying ellipticity, is allowed to propagate, during the course of a classical period they will spread apart. However, because they all have the same classical period they will come back together again at the end of each period. Thus, even at very long times the evolution of the slightly noncircular trajectories can be accurately determined from a local linearization of the dynamics near the circular trajectories in the manner discussed at the end of Sec. II [see Eq. (8)].

The next step is to study the dynamics of circular trajectories as a function of energy. The circular trajectories in the x-y plane can be fully parametrized by the action variable n and the initial angle ϕ_0,

$$r = n^2 \ ,$$
$$\phi = \phi_0 + \frac{1}{n^3}t \ . \tag{12}$$

Consider a set of circular trajectories which start with different values of r but have the same initial value $\phi_0 = 0$, as if they were at the starting line of a race track. As can be seen from Eqs. (12), the trajectories in this "race-track" ensemble with larger r will take longer to cover the same range of angle ϕ than those with smaller r, so there will be a shearing of this ensemble as time increases. If the race-track ensemble is well-localized with values of r near some large $\overline{r}$, the shearing will be small for the first several periods, with the trajectories on the "inside track" gradually creeping ahead of the ones outside. The shearing of the race-track ensemble for relatively short times is displayed in Fig. 2. At these short times, the behavior of the entire race-track ensemble can be accurately described by linearizing the dynamics about the trajectory at the mean energy. A similar linearization of the dynamics about the central trajectory of the circular-orbit ensemble will accurately explain the behavior of the

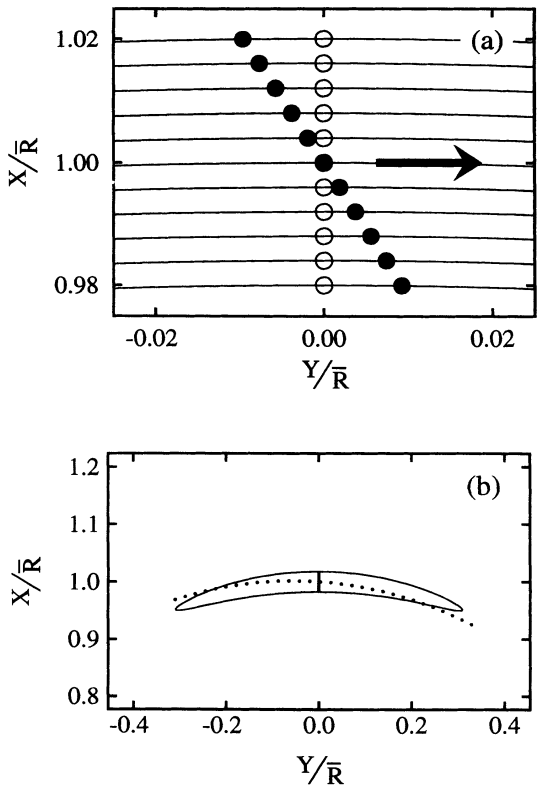

FIG. 2. Shearing of race-track ensemble. (a) Circular trajectories at integer values of $n = 9\,995$ to $10\,005$ ($\overline{n} = 10\,000$), with differences in r exaggerated by a factor of 20. Initially lined up at $t = 0$ (open circles), the trajectories at smaller r move ahead after traveling clockwise for $t = T_{\rm cl}$ (solid circles). (b) In this case a continuous distribution with $\overline{n} = 360$ and $\sigma_n = 10/\pi$ is plotted to scale at $t = 0$ (solid vertical line) and $t = 2T_{\rm cl}$ (dotted line). The solid outline shows the corresponding Gaussian wave-packet contour.

circular-orbit wave packet. Ehrenfest's theorem applies during this range of times, which defines the classical regime of the wave packet's evolution. The extent of this regime has been dubbed the *Ehrenfest time* by Heller and Tomsovic [24].

At much longer times, the trajectories at smaller values of r will lap the ones at larger values of r. The shearing will be so great that the race-track ensemble will be spread out in a large spiral, as illustrated in Fig. 3. At this point the ensemble has spread out so much that trajectories on the inside part of the spiral have gone around the nucleus several times more than those on the outside of the spiral. As mentioned in Sec. II, the partitioning scheme needed for evaluation of the semiclassical correlation function depends on the location of the final state. Hence, for the autocorrelation function it is the intersection of the spiral with the initial Gaussian that is pertinent. Viewing the intersections that the spiral structure makes with the Gaussian wave-packet outline in Fig. 4, the race-track ensemble can be characterized by the different strips, which each represent a set of trajectories that have just completed, or are about to complete, the same number of repetitions of their periods. Each member of one of the strips will differ from any other member of the same strip only by a small increment in energy, and so a linearization of the dynamics about any single member is sufficient to completely determine the evolution of the entire set in the strip.

Keeping in mind that all of the circular trajectories plotted in Fig. 4 left $\phi_0 = 0$ at $t' = 0$, the most symmetric choice of trajectory to represent the strip is the one at $\phi_t = 0$, which will be completing its kth period exactly at time $t' = t$. This trajectory will be defined as the kth *reference trajectory*, and it is determined from

$$kT_k = t \ , \tag{13}$$

where k is an integer and $T_k = 2\pi n_k^3$ is the period of

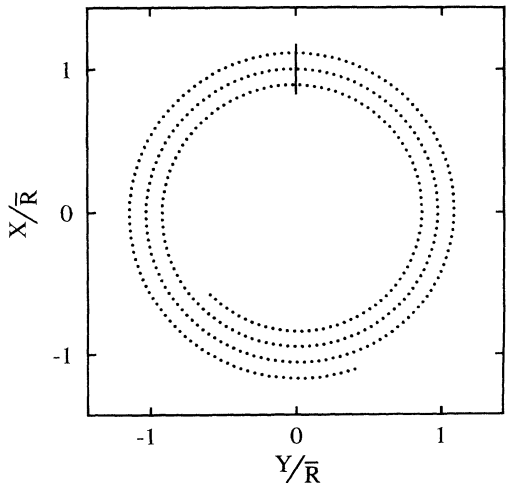

FIG. 3. Spiral formed by race-track ensemble at long times. The initial distribution (solid line) has mean $\overline{n} = 360$ and variance $\sigma_n = 10/\pi$, and the final distribution (dotted line) shows the amount of shear at $t = 60T_{\rm cl}$. The spread in radii is exaggerated by a factor of 10.

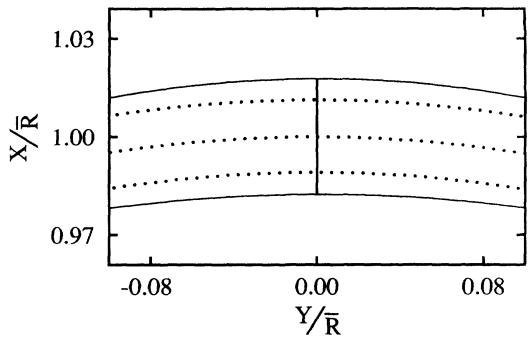

FIG. 4. Intersection of race-track spiral with Gaussian wave packet. Expanded view of the spiral shown in Fig. 3, this time plotted properly scaled. The solid horizontal curves are the visible portions of the Gaussian contour [see Fig. 2(b)], and solid vertical and dotted lines are as in Fig. 3.

the orbit. Here, and for the remainder of the paper, the subscript k on a variable indicates that it is evaluated for the circular trajectory which satisfies the condition (13). The partitioning of the circular race-track trajectories into strips is the same as partitioning them into energy ranges centered at the reference trajectories defined by Eq. (13). The circular-orbit ensemble includes slightly elliptical trajectories as well as circular ones, so we define the kth *partition* to be all circular and almost circular trajectories close in energy to the kth reference trajectory that leave the vicinity of the Gaussian at time $t' = 0$ and return to the vicinity of the Gaussian at time $t' = t$. According to the discussion at the end of Sec. II, these trajectories and their contributions to the semiclassical propagator are obtained from a linearization of the dynamics about the reference trajectory's initial and final positions. This requires the solution to the stability matrix given by Eq. (8) for closed circular orbits in the x-y plane.

It is most appropriate in this case to solve for the stability matrix in polar coordinates,

$$\mathbf{M}_t^k = \left.\frac{\partial(r_t, \theta_t, \phi_t, p_{r_t}, p_{\theta_t}, p_{\phi_t})}{\partial(r_0, \theta_0, \phi_0, p_{r_0}, p_{\theta_0}, p_{\phi_0})}\right|_k . \tag{14}$$

This can be solved analytically for general Kepler trajectories by several methods, but for a full three-dimensional treatment this becomes rather tedious. It is easiest to take a direct approach for the special case of the circular trajectories in the x-y plane. The stability matrix for these trajectories can be easily found by varying the initial conditions $(r_0, \theta_0, \phi_0, p_{r_0}, p_{\theta_0}, p_{\phi_0}) = (n^2, \pi/2, 0, 0, 0, n)$ by an infinitesimal increment in each phase space coordinate, one at a time, and finding the Kepler ellipse that results. Once the perturbed ellipse is found, the change in the phase space coordinates at some later time t is readily determined from the Kepler equations.

This procedure is straightforward, so we just give the final result. For a circular trajectory at a time which is a multiple of its period, the stability matrix has the simple form

$$\mathbf{M}_t^k = \begin{pmatrix} 1 & 0 & 0 & 0 & 0 & 0 \\ 0 & 1 & 0 & 0 & 0 & 0 \\ 0 & 0 & 1 & 0 & 0 & -\Gamma_k^s t \\ 0 & 0 & 0 & 1 & 0 & 0 \\ 0 & 0 & 0 & 0 & 1 & 0 \\ 0 & 0 & 0 & 0 & 0 & 1 \end{pmatrix} . \quad (15)$$

The only nonzero off-diagonal element is $\partial\phi_t/\partial p_{\phi_0}$, and it is proportional to

$$\Gamma_k^s = \frac{3}{n_k^4} , \quad (16)$$

which determines the shearing rate of the nearby trajectories. There is an interesting relationship between this shearing rate and the wave-packet revival period. This will be discussed further in the next section, where the results of this section will be applied in conjunction with the semiclassical method from Sec. II.

V. CIRCULAR-ORBIT AUTOCORRELATION FUNCTIONS

The autocorrelation function of an initially well-localized wave packet captures the most important features of its evolution. As the wave packet slowly decays in the classical regime, the autocorrelation function maps this as a series of spreading peaks centered at the classical period. When the wave packet undergoes fractional revivals, the wave-packet fractions are mapped out as a series of well-localized peaks separated by the relevant fraction of the classical period from one another. Additionally, the Fourier transform of the autocorrelation function yields the eigenvalues of the system over the band of energies covered by the wave packet, but that plays a secondary role here as the primary concern is the dynamics of the system.

The autocorrelation function is also an important physical observable which is more accessible to experiment than the wave function itself. This is because there is a close connection between the autocorrelation function of a Rydberg wave packet and the result of a pump-probe experiment used to excite and detect it. The wave packets excited by short laser pulses are usually radially localized [5–7], but their autocorrelation functions behave very similarly to those of circular-orbit wave packets. This is most easily seen from the eigenstate representation of the autocorrelation function

$$\langle\Psi(0)|\Psi(t)\rangle = \sum_n |a_n|^2 \exp(-i\omega_n t) , \quad (17)$$

where the a_n's have a Gaussian distribution about $\overline{n}$, as indicated in Eq. (9). A wave packet excited from a ground state to, say, the p states of the Rydberg series will populate those states with a distribution in energy similar to what is found in Eq. (9), for a laser pulse with a Gaussian shape. This is because there is a Fourier transform relationship between the laser pulse excitation and the final Rydberg state amplitude distribution [6]. Because the energy level spacing is the same for the p states as it is for the aligned states, the correlation function for the radial wave packet is very close to Eq. (17).

In the classical limit of large $\overline{n}$ and with the condition $\sigma_n \ll \overline{n}$, the levels with significant population satisfy $n - \overline{n} \ll \overline{n}$. Over such a small range of energies in the Rydberg series, the energy levels are spaced approximately like those of a harmonic oscillator with period $T_{\rm cl} = 2\pi\overline{n}^3$ equal to that of the Kepler orbit at the mean energy. The wave-packet autocorrelation is close to that of the harmonic oscillator until times such that the nonlinearity of the energy levels becomes significant, when the wave-packet decay becomes apparent. However, it has been predicted theoretically [5,11,12] and observed experimentally [9] that at times near the so-called *revival* period

$$T_{\rm rev} = \frac{\overline{n}}{3} T_{\rm cl} , \quad (18)$$

the wave packet will approximately regain its original form. Furthermore, at certain fractions of this period the wave packet undergoes fractional revivals [9,11,12]. The rest of this section is devoted to showing how these features can be accurately reproduced semiclassically, without the need for the quantized energy levels.

The semiclassical approximation for the correlation function defined by Eq. (7) is integrated in the Appendix, after linearizing the action R about that of an arbitrary reference trajectory. The resulting expression in Eq. (A11) depends upon the parameters of the initial and final Gaussians, and those of the reference trajectory. As discussed in Sec. IV, each reference trajectory for the autocorrelation function of the circular-orbit wave packets is the kth recurrence of a circular orbit. In Eq. (13) this orbit is defined by $T_k = t/k$, which is more conveniently expressed as a relation for the action variable,

$$n_k = \left(\frac{t}{2\pi k}\right)^{1/3} . \quad (19)$$

As these are closed orbits, the initial and final positions of the trajectory are the same point. This point is chosen to be in the x-y plane with $\phi = \overline{\phi}$, where $\overline{\phi} = 0$ is the center of the wave packet in ϕ; see Eq. (10). This is used, along with $r = n^2$ from Eq. (12), to get

$$\begin{aligned}(r_0, \theta_0, \phi_0, p_{r_0}, p_{\theta_0}, p_{\phi_0}) &= (r_t, \theta_t, \phi_t, p_{r_t}, p_{\theta_t}, p_{\phi_t}) \\ &= (n_k^2, \pi/2, 0, 0, 0, n_k) . \end{aligned} \quad (20)$$

The stability matrix of this reference trajectory is given by Eq. (15), and only depends upon k and n_k, as can be seen from Eqs. (16) and (19). The Maslov index μ_k of the reference trajectory is determined from its conjugate points. For a single repeat of a Kepler orbit there are four conjugate points [19,21], which results in a phase contribution of 2π per orbit repeat.

The initial and final wave packets are identical for an autocorrelation function. The parameters of the Gaussian wave packet are completely specified by its mean position and variance in phase space. The mean phase space coordinates of the circular-orbit wave packet are identical to the initial and final position of the ref-

erence trajectories, except for $\bar{r} = \bar{n}^2$ and $\bar{p}_\phi = \bar{n}$. The wave packet variances are specified by a width matrix. The width matrix of the circular-orbit wave packet is diagonal, and is readily obtained by inspection of Eq. (10),

$$\mathbf{W} = \begin{pmatrix} 1/2\sigma_r^2 & 0 & 0 \\ 0 & 1/2\sigma_\theta^2 & 0 \\ 0 & 0 & 1/2\sigma_\phi^2 \end{pmatrix} . \tag{21}$$

The semiclassical sum for the circular-orbit wave packet autocorrelation function can now be calculated by using Eqs. (15), (16), and (19)–(21) in Eqs. (A9)–(A11) in the Appendix. The final result can be simplified to

$$C_{\rm sc}(t) = \sum_k C_{\rm sc}^k(t) = \sum_k \frac{\sigma_\phi}{\alpha_k} \exp\left(-\frac{(n_k - \bar{n})^2}{\beta_k^2} + iR_k^0 \right) . \tag{22}$$

The full action for the kth reference trajectory is

$$R_k^0 = S_k - E_k t = 2\pi k n_k + \frac{1}{2n_k^2} t \ , \tag{23}$$

and the parameters for the amplitude are

$$\begin{aligned} \alpha_k^2 &= \sigma_\phi^2 - i\chi_k^2 \ , \\ \beta_k^2 &= \frac{1}{\sigma_\phi^2} + i\frac{1}{\chi_k^2} \ , \\ \chi_k^2 &= \frac{\Gamma_k^s}{2} t \ . \end{aligned} \tag{24}$$

The exact quantum autocorrelation function in Eq. (17) and its semiclassical counterpart in Eq. (22) are plotted in Figs. 5 and 6. Their real parts are compared to check the accuracy of the phase as well as the magnitude of the semiclassical approximation. To aid the comparison, the quantity studied is $\overline{C}(t) = e^{i\bar{\omega}t}\langle\Psi(0)|\Psi(t)\rangle \approx e^{i\bar{\omega}t} C_{\rm sc}(t)$, which removes the rapid oscillations. The initial parameters of the wave packet studied in Fig. 5 are chosen such that it remains well-localized for a number of Kepler periods. As can be seen in Fig. 5(a), the semiclassical sum provides a very accurate solution to the autocorrelation function during the initial decay of the wave packet, except for the first recurrence of the wave packet. We note that the semiclassical sum in Eq. (22) does not apply near $t = 0$ because none of the trajectories in the circular-orbit ensemble will have time to complete their orbits. At any time after the initial decay, there is no visible difference between the exact and semiclassical expressions. An example of this is shown in Fig. 5(b), which compares the two expressions near the half revival. Figure 6 examines the accuracy of the semiclassical approximation at the same times as in Fig. 5, but for a wave packet which is initially much better localized in ϕ. This large decrease in width requires a corresponding increase in spread over energy, and as a result the wave packet breaks apart even in its first orbit about the nucleus, and never fully revives. For this wave packet, the semiclassical sum accurately reproduces all of the features of its autocorrelation function, even the recurrence at the first classical period.

It may come as a surprise that the semiclassical ap-

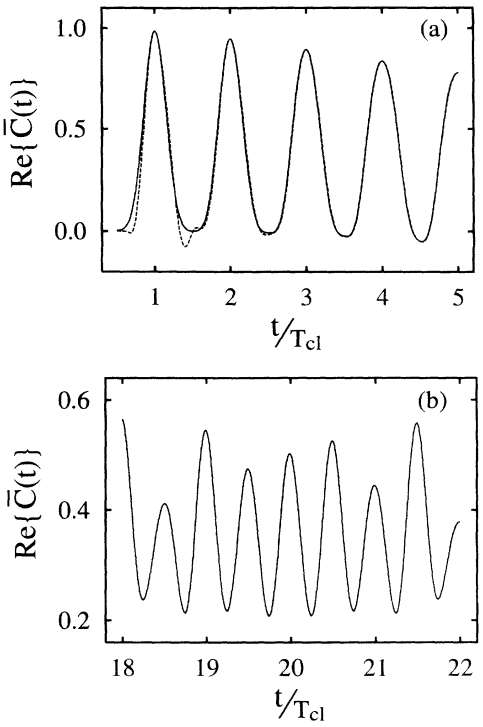

FIG. 5. Accuracy of semiclassical result. The real part of the exact autocorrelation function (solid line) is compared to that of the semiclassical approximation (dashed line). The wave-packet parameters are $\bar{n} = 120$ and $\sigma_\phi = 2\pi/10$. The comparison is during (a) the classical regime (b) the 1/2 revival.

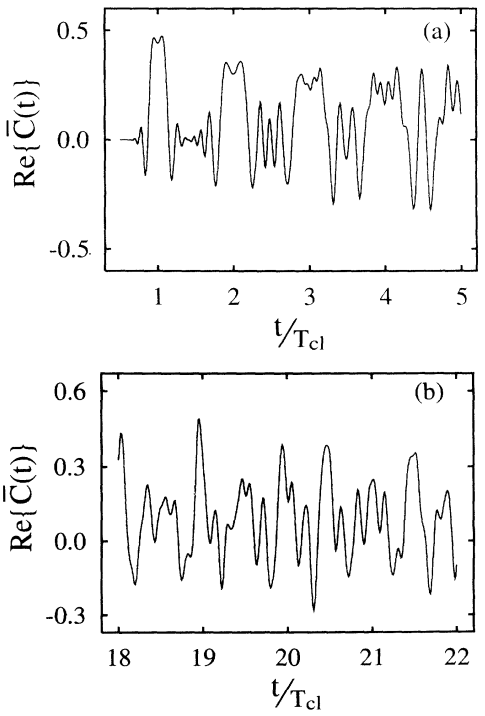

FIG. 6. Accuracy of semiclassical result. The real part of the exact autocorrelation function (solid line) is compared to that of the semiclassical approximation (dashed line). The wave-packet parameters are $\bar{n} = 120$ and $\sigma_\phi = 2\pi/40$. The comparison is during (a) the initial decay (b) the 1/2 revival.

proximation works better at short times for a wave packet which has no classical regime of evolution than for one that does. However, this is not due to errors in the semiclassical propagator, but rather in the way it was approximated with reference orbits. The range of energies spanned by a given ensemble partition increases with σ_ϕ. The accuracy of the linearization of the dynamics about a reference trajectory is only good for a constant range of energies at some given time. Thus, the method is expected to be more accurate for smaller values of σ_ϕ, in agreement with Figs. 5(a) and 6(a). The errors in Fig. 5(a) are most pronounced in the wings of the first recurrence because contributions from the trajectories near the mean energy are more important to the wings of the recurrence than contributions from trajectories far from the mean energy are to the center of the recurrence. The accuracy is still good in any case, but could be improved if we linearized the dynamics about the mean energy circular trajectory at these times. This approach would yield a result which is equivalent to that of Brown [10], and is valid in just those cases where the semiclassical approximation in Eq. (22) works most poorly.

The value of the result in Eq. (22) is not merely its accuracy, but also the insight it provides for the correspondence between the classical dynamics of the system and even the nonclassical features of the wave-packet evolution. The transition from the classical regime to the nonclassical regime has been explained previously in terms of the nature of the energy level spacing [11,12]. The semiclassical sum gives an entirely different perspective on this transition. During the classical regime of evolution, the ensemble of trajectories corresponding to a properly prepared wave packet remains well-localized, only spreading significantly after a number of classical periods. Before this ensemble has spread completely around the orbit, there will be at most one significant reference trajectory contribution in the semiclassical sum in Eq. (22) at any given time, and so there will be no nonclassical interference involved. As soon as the classical ensemble has spread around the orbit, as in Fig. 3, more than one contribution will be involved and the nonclassical interference begins. This rate of spreading is given by the shearing rate $\overline{\Gamma}^s$ near the mean energy trajectory. With the use of Eqs. (18) and (16), this shearing rate can be directly related to the revival period by $\overline{\Gamma}^s = 2\pi/T_{\rm rev}$, yielding a classical explanation for this time scale.

This semiclassical approach permits a more intuitive way of approaching wave-packet dynamics in the correspondence principle limit, because all of the terms involved in the semiclassical sum have a classical origin. Furthermore, the partitioning scheme used to simplify the semiclassical calculation also provides an effective basis for understanding the final result. This is because the partitioning "organizes" the members of the relevant classical ensemble into the essential minimum number of terms needed to fully appreciate the dynamics of the system. The ease with which this technique can be applied to a full three-dimensional calculation in hydrogen is also encouraging because of the continued interest in nonintegrable systems such as the diamagnetic Kepler problem and the microwave ionization of Rydberg atoms, as well as other closely related problems which need a multidimensional treatment.

VI. CONCLUSIONS

We have applied an accurate semiclassical method, based on the Van Vleck–Gutzwiller propagator, to a full three-dimensional calculation for the autocorrelation function of circular-orbit Rydberg wave packets. The result was attained by organizing the relevant classical ensemble into appropriate subsets, and evaluating each of their contributions with a properly chosen reference trajectory. These reference trajectories are the circular Kepler trajectories which have completed some multiple of their period at the time of interest. The shearing rate of these Kepler trajectories was seen to be directly related to the revival period of the wave packets, reflecting the intimate connection between the classical and quantum mechanical dynamics even in the nonclassical regime. The semiclassical approximation that results from the use of these reference trajectories proved to be highly accurate, even for very long times during which nonclassical phenomena are observed. With the semiclassical sum, it is seen that the onset of the nonclassical regime of evolution coincides with the beginning of interferences between classical path amplitudes. This provides an alternative description of the dynamics of localized electron wave packets in hydrogen, and helps lay the foundation for the solution of closely related nonintegrable systems.

ACKNOWLEDGMENTS

We would like to acknowledge helpful communications with Steven Tomsovic, Eric Heller, and Michael Nauenberg. This work has been supported by the Army Research Office.

APPENDIX: LINEARIZED SEMICLASSICAL INTEGRALS

The circular-orbit wave packet in Eq. (10) is a specific example of an N-dimensional Gaussian wave packet of the form

$$\psi_a(\mathbf{q}) = \left[\det\left(\frac{2}{\pi}\mathbf{W}_a\right)\right]^{1/4} \exp\left[\frac{i}{\hbar}\mathbf{p}_a\cdot(\mathbf{q}-\mathbf{q}_a)\right] \times \exp\left[-(\mathbf{q}-\mathbf{q}_a)\cdot\mathbf{W}_a\cdot(\mathbf{q}-\mathbf{q}_a)\right]. \quad \text{(A1)}$$

This Gaussian represents a probability distribution localized about $(\mathbf{q}_a, \mathbf{p}_a)$ in phase space. The $N \times N$ matrix $\mathbf{W}_a$ specifies the width of the Gaussian in configuration space, and is assumed to be symmetric. With wave functions ψ_a and ψ_b having the form given in Eq. (A1), an approximate analytical solution to the correlation function defined by Eq. (7) can be found if the action $R_k(\mathbf{q}, \mathbf{q}'; t)$ is expanded out to second order about the initial and final coordinates of the kth reference trajectory. This expansion results in the *linearized* action

$$R_k^{\rm lin}(\mathbf{q},\mathbf{q}';t) = R_k^0(\mathbf{q}_t,\mathbf{q}_0;t) + \left(\frac{\partial R_k}{\partial \mathbf{q}'}\right)_{\mathbf{q}_0}\cdot(\mathbf{q}'-\mathbf{q}_0) + \left(\frac{\partial R_k}{\partial \mathbf{q}}\right)_{\mathbf{q}_t}\cdot(\mathbf{q}-\mathbf{q}_t) + \frac{1}{2}(\mathbf{q}'-\mathbf{q}_0)\cdot\left(\frac{\partial^2 R_k}{\partial \mathbf{q}'^2}\right)_{\mathbf{q}_0}\cdot(\mathbf{q}'-\mathbf{q}_0)$$
$$+\frac{1}{2}(\mathbf{q}-\mathbf{q}_t)\cdot\left(\frac{\partial^2 R_k}{\partial \mathbf{q}^2}\right)_{\mathbf{q}_t}\cdot(\mathbf{q}-\mathbf{q}_t) + (\mathbf{q}-\mathbf{q}_t)\cdot\left(\frac{\partial^2 R_k}{\partial \mathbf{q}\partial \mathbf{q}'}\right)_{\mathbf{q}_t,\mathbf{q}_0}\cdot(\mathbf{q}'-\mathbf{q}_0)\quad , \tag{A2}$$

where $\mathbf{q}_0$ and $\mathbf{q}_t$ are the initial and final positions of the reference trajectory, respectively.

Using Eq. (A2) in Eq. (7) leads to two N-dimensional Gaussian integrals. To evaluate the integrals, the derivatives of the action integral need to be put into a useful form. The first derivatives are given, from elementary classical mechanics [21], by

$$\left(\frac{\partial R_k}{\partial \mathbf{q}'}\right)_{\mathbf{q}_0} = -\mathbf{p}_0 \quad , \qquad \left(\frac{\partial R_k}{\partial \mathbf{q}}\right)_{\mathbf{q}_t} = \mathbf{p}_t \ . \tag{A3}$$

The second derivatives are solved for in terms of the elements of the stability matrix, defined by

$$\begin{pmatrix}\delta\mathbf{q}_t\\ \delta\mathbf{p}_t\end{pmatrix} = \mathbf{M}_t^k\begin{pmatrix}\delta\mathbf{q}_0\\ \delta\mathbf{p}_0\end{pmatrix}, \tag{A4}$$

where $(\delta\mathbf{q}_0,\delta\mathbf{p}_0)$ are small deviations about the initial conditions of the reference trajectory and $(\delta\mathbf{q}_t,\delta\mathbf{p}_t)$ are the resulting deviations at the final time t. Decomposing the stability matrix into four $N\times N$ blocks

$$\mathbf{M}_t^k = \begin{pmatrix}\dfrac{\partial\mathbf{q}_t}{\partial\mathbf{q}_0} & \dfrac{\partial\mathbf{q}_t}{\partial\mathbf{p}_0}\\ \dfrac{\partial\mathbf{p}_t}{\partial\mathbf{q}_0} & \dfrac{\partial\mathbf{p}_t}{\partial\mathbf{p}_0}\end{pmatrix} = \begin{pmatrix}\mathbf{A} & \mathbf{B}\\ \mathbf{C} & \mathbf{D}\end{pmatrix}, \tag{A5}$$

the second derivatives of the action integral work out to

$$\left(\frac{\partial^2 R_k}{\partial \mathbf{q}^2}\right)_{\mathbf{q}_t} = \mathbf{D}\mathbf{B}^{-1}\ ,$$
$$\left(\frac{\partial^2 R_k}{\partial \mathbf{q}'^2}\right)_{\mathbf{q}_0} = \mathbf{B}^{-1}\mathbf{A}\ , \tag{A6}$$
$$\left(\frac{\partial^2 R_k}{\partial \mathbf{q}\partial \mathbf{q}'}\right)_{\mathbf{q}_t,\mathbf{q}_0} = -(\mathbf{B}^T)^{-1}\ ,$$

where use was made of the fact that $\mathbf{M}_t^k$ is a symplectic matrix [17]. The double integral in Eq. (7) is now approximated by

$$C_{ba}^k(t) \approx \left[\det(2\pi i\hbar\mathbf{B})\right]^{-1/2}\iint d\mathbf{q}\,d\mathbf{q}'\,\psi_b^*(\mathbf{q})\,\psi_a(\mathbf{q}')$$
$$\times\exp\left(\frac{i}{\hbar}R_k^{\rm lin}(\mathbf{q},\mathbf{q}';t) - i\frac{\pi}{2}\mu_k\right), \tag{A7}$$

which is a pair of Gaussian integrals; see Eq. (A2) for the linearized action integral. This can be evaluated for the general case, but it simplifies considerably if the matrices $\mathbf{A}$, $\mathbf{B}$, $\mathbf{C}$, $\mathbf{D}$, and $\mathbf{W}_a = \mathbf{W}_b = \mathbf{W}_\sigma^{-2}/2$ are diagonal.

The new matrix $\mathbf{W}_\sigma$ takes the diagonal form

$$\mathbf{W}_\sigma = \begin{pmatrix}\sigma_1 & 0 & \cdots & 0\\ 0 & \sigma_2 & \cdots & 0\\ \vdots & \vdots & \ddots & \vdots\\ 0 & 0 & \cdots & \sigma_n\end{pmatrix}. \tag{A8}$$

The following matrix definitions are useful:

$$\mathbf{Y}_0 = \mathbf{A}+\mathbf{D}+\mathbf{V}\mathbf{B}+\mathbf{C}\mathbf{V}^{-1}\ ,$$
$$\mathbf{Y}_1 = \mathbf{A}+\mathbf{V}\mathbf{B}\quad ,\quad \mathbf{Y}_2 = \mathbf{D}+\mathbf{C}\mathbf{V}^{-1}\ , \tag{A9}$$
$$\mathbf{Y}_3 = \mathbf{A}+\mathbf{C}\mathbf{V}^{-1}\quad ,\quad \mathbf{Y}_4 = \mathbf{D}+\mathbf{V}\mathbf{B}\ ,$$

with $\mathbf{V} = i\hbar\mathbf{W}_\sigma^{-2}$. Also needed are the scaled variables,

$$\tilde{\mathbf{q}}_0 = \mathbf{W}_\sigma^{-1}\cdot(\mathbf{q}_0-\mathbf{q}_a)\quad ,\quad \tilde{\mathbf{p}}_0 = \mathbf{W}_\sigma\cdot(\mathbf{p}_0-\mathbf{p}_a)/\hbar\ ,$$
$$\tilde{\mathbf{q}}_t = \mathbf{W}_\sigma^{-1}\cdot(\mathbf{q}_t-\mathbf{q}_b)\quad ,\quad \tilde{\mathbf{p}}_t = \mathbf{W}_\sigma\cdot(\mathbf{p}_t-\mathbf{p}_b)/\hbar\ . \tag{A10}$$

Performing the integrals in Eq. (A7) yields

$$C_{ba}^k(t) = \left[\det(\mathbf{Y}_0/2)\right]^{-1/2}\exp\Big\{\frac{i}{\hbar}\Big[R_k^0+\mathbf{p}_a\cdot(\mathbf{q}_0-\mathbf{q}_a)-\mathbf{p}_b\cdot(\mathbf{q}_t-\mathbf{q}_b)\Big]-i\frac{\pi}{2}\mu_k$$
$$-\frac{1}{2}\Big(\tilde{\mathbf{q}}_0\cdot\mathbf{Y}_3\mathbf{Y}_0^{-1}\cdot\tilde{\mathbf{q}}_0+\tilde{\mathbf{p}}_0\cdot\mathbf{Y}_4\mathbf{Y}_0^{-1}\cdot\tilde{\mathbf{p}}_0+\tilde{\mathbf{q}}_t\cdot\mathbf{Y}_2\mathbf{Y}_0^{-1}\cdot\tilde{\mathbf{q}}_t+\tilde{\mathbf{p}}_t\cdot\mathbf{Y}_1\mathbf{Y}_0^{-1}\cdot\tilde{\mathbf{p}}_t\Big)$$
$$+i\big(\tilde{\mathbf{q}}_0\cdot\mathbf{Y}_4\mathbf{Y}_0^{-1}\cdot\tilde{\mathbf{p}}_0-\tilde{\mathbf{q}}_t\cdot\mathbf{Y}_1\mathbf{Y}_0^{-1}\cdot\tilde{\mathbf{p}}_t\big)+(\tilde{\mathbf{q}}_0+i\tilde{\mathbf{p}}_0)\cdot\mathbf{Y}_0^{-1}\cdot(\tilde{\mathbf{q}}_t-i\tilde{\mathbf{p}}_t)\Big\}\ . \tag{A11}$$

[1] E. Schrödinger, Naturwissenschaften **14**, 664 (1926); in *Letters on Wave Mechanics*, edited by K. Prizibram (Philosophical Library, New York, 1967).

[2] J. Mostowski, Lett. Math. Phys. **2**, 1 (1977); D. Bhaumik, B. Dutta-Roy, and G. Ghosh, J. Phys. A **19**, 1355 (1986).

[3] M. M. Nieto, Phys. Rev. D **22**, 391 (1980); V. P. Gutschick and M. M. Nieto, *ibid.* **22**, 403 (1980).

[4] M. Nauenberg, Phys. Rev. A **40**, 1133 (1989).

[5] J. Parker and C. R. Stroud, Jr., Phys. Rev. Lett. **56**, 716 (1986).

[6] G. Alber and P. Zoller, Phys. Rep. **199**, 231 (1991).
[7] A. ten Wolde, L. D. Noordam, A. Lagendijk, and H. B. van Linden van den Heuvell, Phys. Rev. Lett. **61**, 2099 (1988); J. A. Yeazell, M. Mallalieu, J. Parker, and C. R. Stroud, Jr., Phys. Rev. A **40**, 5040 (1989).
[8] J. A. Yeazell and C. R. Stroud, Jr., Phys. Rev. A **35**, 2806 (1987); Phys. Rev. Lett. **60**, 1494 (1988).
[9] J. A. Yeazell, M. Mallalieu, and C. R. Stroud, Jr., Phys. Rev. Lett. **64**, 2007 (1990); J. A. Yeazell and C. R. Stroud, Jr., Phys. Rev. A **43**, 5153 (1991); D. R. Meacher, P. E. Meyler, I. G. Hughes, and P. Ewart, J. Phys. B **24**, L63 (1991).
[10] L. S. Brown, Am. J. Phys. **41**, 525 (1973).
[11] Z. D. Gaeta and C. R. Stroud, Jr., Phys. Rev. A **42**, 6308 (1990).
[12] I. Sh. Averbukh and N. F. Perelman, Phys. Lett. A **139**, 449 (1989).
[13] M. Nauenberg, J. Phys. B **23**, L385 (1990).
[14] S. Tomsovic and E. J. Heller, Phys. Rev. Lett. **67**, 664 (1991); Phys. Rev. E **47**, 282 (1993).
[15] S. Tomsovic and E. J. Heller, Phys. Rev. Lett. **70**, 1405 (1993).
[16] E. J. Heller, in *Chaos and Quantum Physics*, Les Houches Session LII, 1989, edited by M. J. Giannoni, A. Voros, and J. Zinn-Justin (Elsevier Science Publishers B.V., Amsterdam, 1991).
[17] R. G. Littlejohn, Phys. Rep. **138**, 193 (1986).
[18] J. H. Van Vleck, Proc. Nat. Acad. Sci. USA **14**, 178 (1928).
[19] M. C. Gutzwiller, J. Math. Phys. **8**, 1979 (1967); **10**, 1004 (1969); **11**, 1791 (1970); **12**, 343 (1971).
[20] I. M. Suarez Barnes, M. Nauenberg, M. Nockelby, and S. Tomsovic, Phys. Rev. Lett. **71**, 1961 (1993).
[21] M. C. Gutzwiller, *Chaos in Classical and Quantum Mechanics* (Springer-Verlag, New York, 1990).
[22] Gutzwiller [19,21] found the classical limit of the Feynman propagator, generalizing the result of Van Vleck [18] to include the effects of multiple classical paths and conjugate points. One of the best introductions to the Feynman propagator can be found in R. P. Feynman and A. R. Hibbs, *Quantum Mechanics and Path Integrals* (McGraw-Hill, New York, 1965). A nice treatment of the WKB approximation to the Feynman propagator is given in L. S. Schulman, *Techniques and Applications of Path Integration* (Wiley-Interscience, New York, 1981).
[23] A. M. Ozorio de Almeida, *Hamiltonian Systems: Chaos and Quantization* (Cambridge University Press, New York, 1988).
[24] E. J. Heller and S. Tomsovic, Phys. Today **46** (7), 38 (1993).